Instability of asymmetric nuclear matter in the extended Zimanyi-Moszkowski model

K. Miyazaki*

Abstract

We have investigated the unstable spinodal region of asymmetric nuclear matter in the extended Zimanyi-Moszkowski (EZM) model. It is found that the model produces larger spinodal region, higher upper-density boundary and maximum asymmetry, than the familiar nonlinear Walecka model. This is due to the renormalized vector-meson coupling constants in the EZM model.

Recent experimental developments of nuclear multifragmentation reaction have provided valuable information [1] on the liquid-gas phase transition and the critical phenomena in nuclear matter. The nuclear multifragmentation is considered as the spinodal decomposition [2-4]. A hot homogeneous nuclear matter, which is produced by high-energy heavy-ion reaction, expands due to thermal pressure and cools off below the critical temperature, and then falls into unstable spinodal region. Because of density fluctuations, a homogeneous system converts into a mixed-phase state that consists of droplets surrounded by nuclear gas.

In this respect, there are renewed theoretical interests [5-10] on the spinodal instability in nuclear matter. The investigations of Refs. [5], [7] and [9] are based on the nonlinear Walecka (NLW) model of relativistic mean-field (RMF) theory [11]. The NLW model has been most widely used in the investigations of nuclear matter, finite nuclei, strange hadronic matter and neutron stars. Most of their calculations did not take into account the isovector-scalar meson δ that has significant effect to split the effective masses of proton and neutron in the medium and alter the symmetry energy of asymmetric nuclear matter [12], although the recent works [7] and [9] considered the effect. We further have to stress that the NLW model [5] cannot reproduce the empirical value of the critical temperature [13] for nuclear matter. Recently, the author has developed the extended Zimanyi-Moszkowski (EZM) model [14] and applied it to warm symmetric nuclear matter [15]. The model has succeeded to reproduce the empirical values of the critical temperature [13] and critical exponents [2] of nuclear matter in contrast to the NLW model. It is therefore valuable to investigate the spinodal instability of asymmetric nuclear matter in the EZM model.

*E-mail : miyazakiro@rio.odn.ne.jp

The EZM model for cold asymmetric nuclear matter taking into account δ meson has already been developed in Ref. [16]. In the present work, we will extend it to finite temperature. The thermodynamic potential per volume $\tilde{\Omega} \equiv \Omega/V$ of asymmetric nuclear matter at temperature T is

$$\begin{aligned}\tilde{\Omega} &= \frac{1}{2}\, m_\sigma^2 \left\langle \sigma \right\rangle^2 + \frac{1}{2}\, m_\delta^2 \left\langle \delta_3 \right\rangle^2 - \frac{1}{2}\, m_\omega^2 \left\langle \omega_0 \right\rangle^2 - \frac{1}{2}\, m_\rho^2 \left\langle \rho_{03} \right\rangle^2 \\ &\quad - \gamma\, k_B T \sum_{i=p,n} \int_0^\infty \frac{d^3\mathbf{k}}{(2\pi)^3} \left\{ \ln\left[1+\exp\left(\frac{\nu_i - E_{ki}^*}{k_B T}\right)\right] + \ln\left[1+\exp\left(\frac{-\nu_i - E_{ki}^*}{k_B T}\right)\right] \right\},\end{aligned} \tag{1}$$

where k_B is the Boltzmann constant and $E_{ki}^* = (\mathbf{k}^2 + M_i^{*2})^{1/2}$ with the effective mass M_i^* of a proton or neutron in the medium. The spin degeneracy factor γ is equal to 2. The ν_i is defined by the chemical potential μ_i and the vector potential V_{0i} of a proton or neutron as

$$\nu_i = \mu_i - V_{0i}. \tag{2}$$

The scalar mean-field $\langle\sigma\rangle$ is determined [16] from the effective masses by

$$\left\langle \sigma \right\rangle = \frac{\left(1-m_p^*\right) g_{nn\delta}^* + \left(1-m_n^*\right) g_{pp\delta}^*}{g_{pp\sigma}^* g_{nn\delta}^* + g_{nn\sigma}^* g_{pp\delta}^*} M, \tag{3}$$

where M is the free nucleon mass and $M_i^* = m_i^* M$. Similarly, the $\langle\delta_3\rangle$ is determined [16] by

$$\left\langle \delta_3 \right\rangle = \frac{\left(1-m_p^*\right) g_{nn\sigma}^* - \left(1-m_n^*\right) g_{pp\sigma}^*}{g_{pp\sigma}^* g_{nn\delta}^* + g_{nn\sigma}^* g_{pp\delta}^*} M. \tag{4}$$

On the other hand, the vector mean-field $\langle\omega_0\rangle$ is determined [16] from the vector potentials as

$$\left\langle \omega_0 \right\rangle = \frac{g_{nn\rho}^* v_{0p} + g_{pp\rho}^* v_{0n}}{g_{pp\omega}^* g_{nn\rho}^* + g_{nn\omega}^* g_{pp\rho}^*} M, \tag{5}$$

where $V_{0i} = v_{0i} M$. Similarly, the $\langle\rho_{03}\rangle$ is determined [16] from

$$\left\langle \rho_{03} \right\rangle = \frac{g_{nn\omega}^* v_{0p} - g_{pp\omega}^* v_{0n}}{g_{pp\omega}^* g_{nn\rho}^* + g_{nn\omega}^* g_{pp\rho}^*} M. \tag{6}$$

The renormalized meson coupling constants [16] are

$$g_{pp(nn)\Pi}^* = h_{pp(nn)\Pi}^*\, g_{NN\Pi} \quad (\Pi = \sigma,\ \omega,\ \delta,\ \rho), \tag{7}$$

$$h_{pp\sigma(\omega)}^* = (1-\lambda) + \lambda\, m_p^*, \tag{8}$$

$$h_{nn\sigma(\omega)}^* = (1-\lambda) + \lambda\, m_n^*, \tag{9}$$

$$h_{pp\delta(\rho)}^* = (1-\lambda) + \lambda \left(2m_n^* - m_p^*\right), \tag{10}$$

$$h^*_{nn\delta(\rho)} = (1-\lambda) + \lambda\left(2m^*_p - m^*_n\right), \tag{11}$$

with

$$\lambda = 1/3. \tag{12}$$

It is noted that $\lambda = 0$ corresponds to the Walecka model [11].

Then, the effective mass m^*_i and the vector potential v_{0i} are determined from extremizing the thermodynamical potential $\tilde{\Omega}$ by them. We have

$$\frac{\rho_{Bp}}{M} - \left(\frac{m_\omega}{g_{NN\omega}}\right)^2 \frac{\left(h^*_{nn\rho}v_{0p} + h^*_{pp\rho}v_{0n}\right)h^*_{nn\rho}}{D^2} - \left(\frac{m_\rho}{g_{NN\rho}}\right)^2 \frac{\left(h^*_{nn\omega}v_{0p} - h^*_{pp\omega}v_{0n}\right)h^*_{nn\omega}}{D^2} = 0, \tag{13}$$

$$\frac{\rho_{Bn}}{M} - \left(\frac{m_\omega}{g_{NN\omega}}\right)^2 \frac{\left(h^*_{nn\rho}v_{0p} + h^*_{pp\rho}v_{0n}\right)h^*_{pp\rho}}{D^2} + \left(\frac{m_\rho}{g_{NN\rho}}\right)^2 \frac{\left(h^*_{nn\omega}v_{0p} - h^*_{pp\omega}v_{0n}\right)h^*_{pp\omega}}{D^2} = 0, \tag{14}$$

$$\begin{aligned}
&\frac{\rho_{Sp}}{M} + \left(\frac{m_\sigma}{g_{NN\sigma}}\right)^2 \frac{A^{(0)}\left(A^{(1)}_p C^{(0)} - A^{(0)}C^{(1)}_p\right)}{\left(C^{(0)}\right)^3} + \left(\frac{m_\delta}{g_{NN\delta}}\right)^2 \frac{B^{(0)}\left(C^{(0)} - B^{(0)}C^{(1)}_p\right)}{\left(C^{(0)}\right)^3} \\
&+\lambda\left(\frac{m_\omega}{g_{NN\omega}}\right)^2 \frac{h^*_{nn\rho}v_{0p} + h^*_{pp\rho}v_{0n}}{D^3}\left[\left({h^*_{nn\rho}}^2 - 2h^*_{nn\omega}h^*_{pp\rho} - h^*_{nn\omega}h^*_{nn\rho}\right)v_{0p}\right. \\
&\qquad\left. + \left(h^*_{pp\omega}h^*_{nn\rho} + h^*_{pp\rho}h^*_{nn\rho} + 2h^*_{pp\omega}h^*_{pp\rho}\right)v_{0n}\right] \\
&+\lambda\left(\frac{m_\rho}{g_{NN\rho}}\right)^2 \frac{h^*_{nn\omega}v_{0p} - h^*_{pp\omega}v_{0n}}{D^3}\left[h^*_{nn\omega}\left(h^*_{nn\rho} + 2h^*_{pp\omega} - h^*_{nn\omega}\right)v_{0p}\right. \\
&\qquad\left. + \left(h^*_{nn\omega}h^*_{pp\rho} - 2{h^*_{pp\omega}}^2 + h^*_{pp\omega}h^*_{nn\omega}\right)v_{0n}\right] = 0,
\end{aligned} \tag{15}$$

$$\begin{aligned}
&\frac{\rho_{Sn}}{M} + \left(\frac{m_\sigma}{g_{NN\sigma}}\right)^2 \frac{A^{(0)}\left(A^{(1)}_n C^{(0)} - A^{(0)}C^{(1)}_n\right)}{\left(C^{(0)}\right)^3} - \left(\frac{m_\delta}{g_{NN\delta}}\right)^2 \frac{B^{(0)}\left(C^{(0)} + B^{(0)}C^{(1)}_n\right)}{\left(C^{(0)}\right)^3} \\
&+\lambda\left(\frac{m_\omega}{g_{NN\omega}}\right)^2 \frac{h^*_{nn\rho}v_{0p} + h^*_{pp\rho}v_{0n}}{D^3}\left[\left(h^*_{nn\rho}h^*_{nn\omega} + 2h^*_{nn\omega}h^*_{nn\rho} + h^*_{pp\rho}h^*_{nn\rho}\right)v_{0p}\right. \\
&\qquad\left. + \left({h^*_{pp\rho}}^2 - h^*_{pp\omega}h^*_{pp\rho} - 2h^*_{pp\omega}h^*_{nn\rho}\right)v_{0n}\right] \\
&+\lambda\left(\frac{m_\rho}{g_{NN\rho}}\right)^2 \frac{h^*_{nn\omega}v_{0p} - h^*_{pp\omega}v_{0n}}{D^3}\left[\left(2{h^*_{nn\omega}}^2 - h^*_{pp\omega}h^*_{nn\omega} - h^*_{pp\omega}h^*_{nn\rho}\right)v_{0p}\right. \\
&\qquad\left. + h^*_{pp\omega}\left(h^*_{pp\omega} - h^*_{pp\rho} - 2h^*_{nn\omega}\right)v_{0n}\right] = 0,
\end{aligned} \tag{16}$$

where the quantities A, B, C and D are defined by

$$A^{(0)} = h^*_{nn\delta}\left(m^*_p - 1\right) + h^*_{pp\delta}\left(m^*_n - 1\right), \tag{17}$$

$$B^{(0)} = h^*_{nn\sigma}\left(m^*_p - 1\right) - h^*_{pp\sigma}\left(m^*_n - 1\right), \tag{18}$$

$$C^{(0)} = h^*_{pp\sigma}h^*_{nn\delta} + h^*_{nn\sigma}h^*_{pp\delta}, \tag{19}$$

$$A^{(1)}_p = (1-\xi) + \xi\left(2m^*_p - m^*_n\right), \tag{20}$$

$$C^{(1)}_p = \xi\, h^*_{nn\delta}, \tag{21}$$

$$A^{(1)}_n = (1-\xi) + \xi\left(2m^*_n - m^*_p\right), \tag{22}$$

$$C^{(1)}_n = \xi\, h^*_{pp\delta}, \tag{23}$$

$$D = h^*_{pp\omega}h^*_{nn\rho} + h^*_{nn\omega}h^*_{pp\rho}, \tag{24}$$

with $\xi \equiv 2\lambda$.

The baryon and scalar densities are defined by

$$\rho_{Bi} = \gamma \int_0^\infty \frac{d^3\mathbf{k}}{(2\pi)^3}\left[n_{ki}(T) - \bar{n}_{ki}(T)\right], \tag{25}$$

$$\rho_{Si} = \gamma \int_0^\infty \frac{d^3\mathbf{k}}{(2\pi)^3}\frac{M^*_i}{E^*_{ki}}\left[n_{ki}(T) + \bar{n}_{ki}(T)\right], \tag{26}$$

where the Fermi-Dirac distribution functions of nucleon and antinucleon are

$$n_{ki}(T) = \left[1+\exp\left(\frac{E^*_{ki} - \nu_i}{k_B T}\right)\right]^{-1}, \tag{27}$$

$$\bar{n}_{ki}(T) = \left[1+\exp\left(\frac{E^*_{ki} + \nu_i}{k_B T}\right)\right]^{-1}. \tag{28}$$

Given the baryon density ρ_{Bi} and the temperature T, Eqs. (13)-(16) and (25) have to be solved numerically utilizing 6-dimensional Newton-Raphson method so that the effective masses m^*_p and m^*_n, the vector potentials v_{0p} and v_{0n}, and the chemical potentials μ_p and μ_n are determined selfconsistently. Once the chemical potentials are determined, we can evaluate the stability (or metastability) condition for asymmetric nuclear matter [7-9]:

$$-\left(\frac{\partial P}{\partial \rho_B}\right)_{T,a}\left(\frac{\partial \mu_p}{\partial\, a}\right)_{T,P} = \left(\frac{\partial P}{\partial\, a}\right)_{T,\rho_B}\left(\frac{\partial \mu_p}{\partial \rho_B}\right)_{T,a} - \left(\frac{\partial P}{\partial \rho_B}\right)_{T,a}\left(\frac{\partial \mu_p}{\partial\, a}\right)_{T,\rho_B} > 0, \tag{29}$$

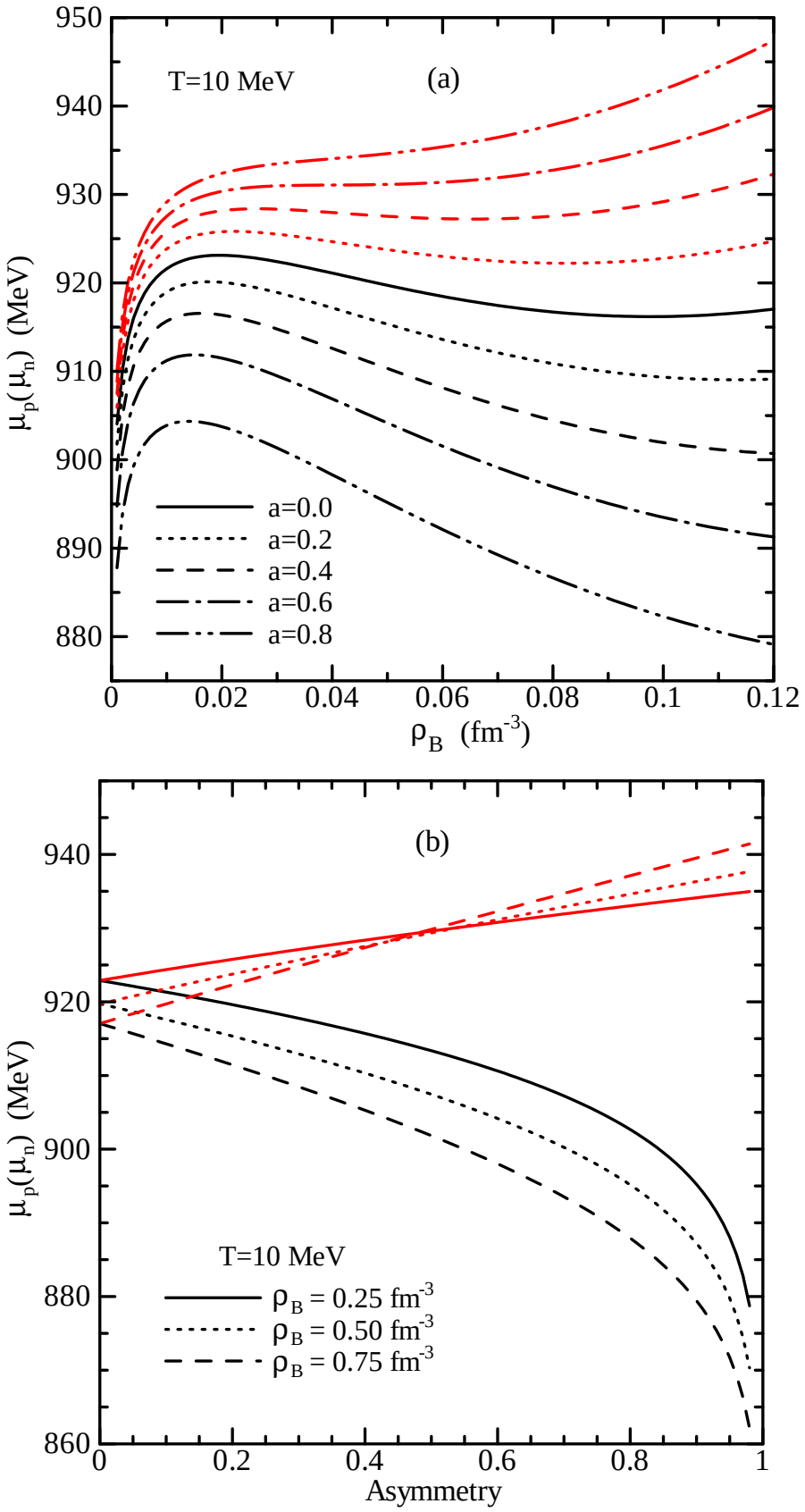

Figure 1: (a) The chemical potentials of proton (black curves) and neutron (red curves) as functions of the total baryon density for the asymmetry $a = 0.0 \sim 0.8$ at $T = 10\,\mathrm{MeV}$. (b) The chemical potentials as functions of the asymmetry for $\rho_B = 0.25$, 0.50 and $0.75\,\mathrm{fm}^{-3}$.

where $\rho_B = \rho_{Bp} + \rho_{Bn}$ is the total baryon density and $a = \left(\rho_{Bn} - \rho_{Bp}\right)/\rho_B$ is the asymmetry. The derivatives of the pressure P are calculated using the Gibbs-Duhem relation:

$$\left(\frac{\partial P}{\partial \rho_B}\right)_{T,a} = \sum_{i=p,n} \rho_{Bi} \left(\frac{\partial \mu_i}{\partial \rho_B}\right)_{T,a}, \tag{30}$$

$$\left(\frac{\partial P}{\partial\, a}\right)_{T,\rho_B} = \sum_{i=p,n} \rho_{Bi} \left(\frac{\partial \mu_i}{\partial\, a}\right)_{T,\rho_B}. \tag{31}$$

Employing the isoscalar meson coupling constants given in Ref. [14] and the isovector meson coupling constants $\left(g_{NN\delta}/m_\delta\right)^2 = 0.39\,\mathrm{fm}^2$ and $\left(g_{NN\rho}/m_\rho\right)^2 = 0.82\,\mathrm{fm}^2$ (hereafter referred to as the coupling set 1) from Bonn A potential [17], Figs. 1(a) and (b) calculate μ_p (black curves) and μ_n (red curves) as functions of ρ_B for several asymmetries and as functions of asymmetry for several densities at $T = 10\,\mathrm{MeV}$. (Of course $\mu_p = \mu_n$ at $a = 0.0$.) From these results we can calculate $\left(\partial\mu_i/\partial\rho_B\right)_{T,a}$ and $\left(\partial\mu_i/\partial\, a\right)_{T,\rho_B}$ in Eqs. (29)-(31). Then, Fig. 2 shows $-\left(\partial P/\partial\rho_B\right)_{T,a}\left(\partial\mu_p/\partial\, a\right)_{T,P}$ as a function of ρ_B. The region of negative values is just the unstable spinodal region. It becomes narrower as the asymmetry grows because the larger breaking of symmetry make the system more disordered. It is also seen that the minimum of the curve shifts to lower density as the asymmetry increases. In other words, the upper-density boundary of the spinodal region decreases faster than its lower-density boundary increases. This is because the effects of isovector mesons are larger at higher density. Figure 3 shows the resultant spinodal regions in the density-asymmetry plain at $T = 0$, 8, 10, 12 and 14 MeV. Because the system generally becomes more disordered at higher temperature, the spinodal region becomes smaller.

The symmetry energy of nuclear matter using the coupling set 1 is $E_s = 24.6\,\mathrm{MeV}$ that is lower than its empirical value $30 \pm 4\,\mathrm{MeV}$. This is due to the relatively weak $NN\rho$ coupling. In order to investigate the effect of the symmetry energy, we calculate the spinodal region using $\left(g_{NN\delta}/m_\delta\right)^2 = 0.39\,\mathrm{fm}^2$ but stronger $NN\rho$ coupling $\left(g_{NN\rho}/m_\rho\right)^2 = 1.432\,\mathrm{fm}^2$ (referred to as the set 2) that produces the symmetry energy $E_s = 32.0\,\mathrm{MeV}$. Moreover, in order to investigate the effect of ambiguity in the isovector coupling constants, we calculate using stronger $NN\delta$ coupling $\left(g_{NN\delta}/m_\delta\right)^2 = 1.0\,\mathrm{fm}^2$ and much stronger$NN\rho$ coupling $\left(g_{NN\rho}/m_\rho\right)^2 = 1.888\,\mathrm{fm}^2$ (referred to as the set 3) that also reproduce $E_s = 32.0\,\mathrm{MeV}$. The results at $T = 10\,\mathrm{MeV}$ are shown in Fig. 4. The solid, dashed and dotted curves are the results using the set 1, 2 and 3, respectively. In the comparison of the set 1 with the set 2, we can see that the maximum asymmetry of spinodal region becomes lower for higher symmetry energy while the spinodal region in $a < 0.4$ is not affected by the difference of the energy. In the comparison of the set 2 with the set 3, it is seen that for a fixed value of the symmetry energy the differences of the isovector coupling constants have little effect on the spinodal region.

The above results can be recognized as follows. For a fixed weak $NN\delta$ coupling constant in the sets 1 and 2, the stronger $NN\rho$ coupling constant in the set 2 produces

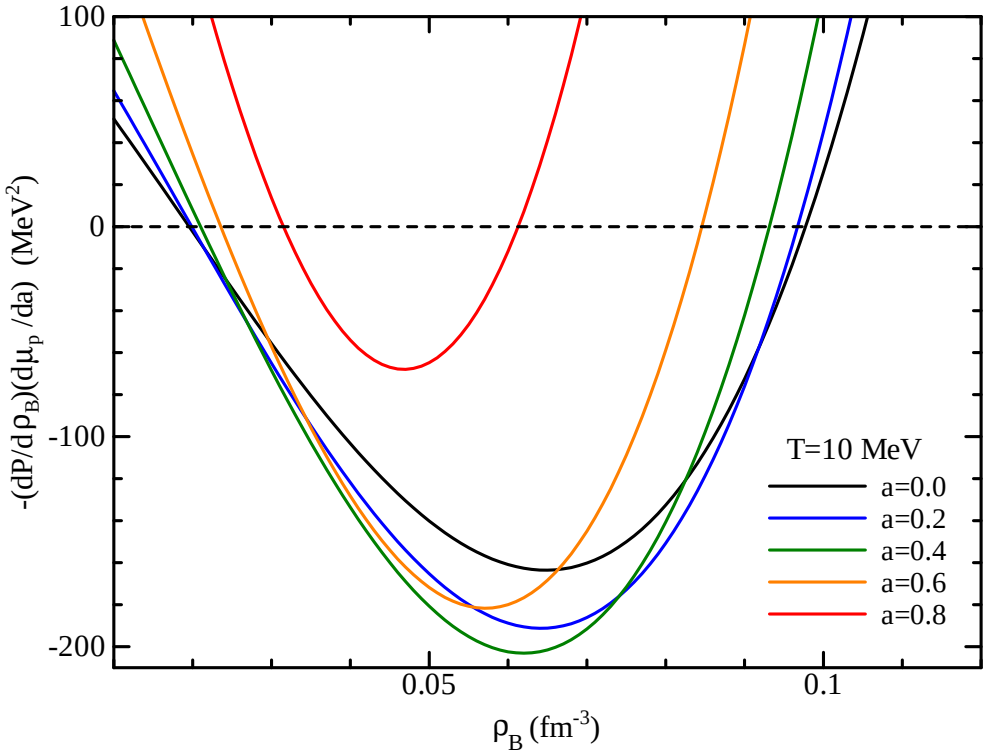

Figure 2: $-\left(\partial P/\partial\rho_B\right)_{T,a}\left(\partial\mu_p/\partial\, a\right)_{T,P}$ as a function of the total baryon density for $a = 0.0 \sim 0.8$ at $T = 10\,\mathrm{MeV}$.

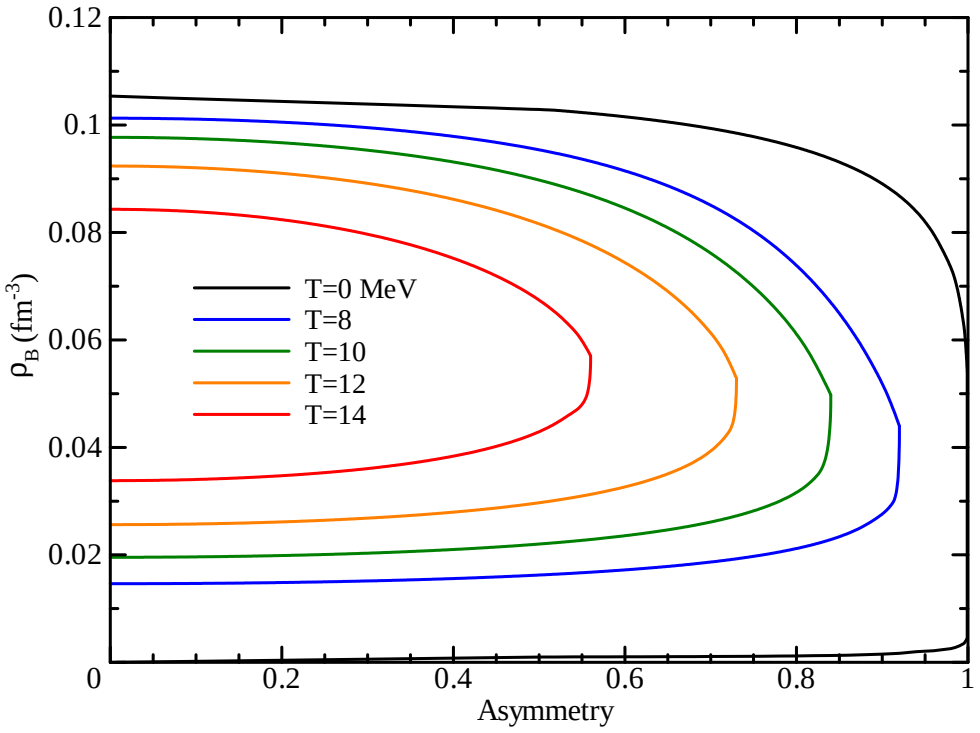

Figure 3: The spinodal regions in the density-asymmetry plain at $T = 0$, 8, 10, 12 and 14 MeV. The instability regions lie inside the curves. The isovector meson coupling constants are from Bonn A potential of Ref. [17].

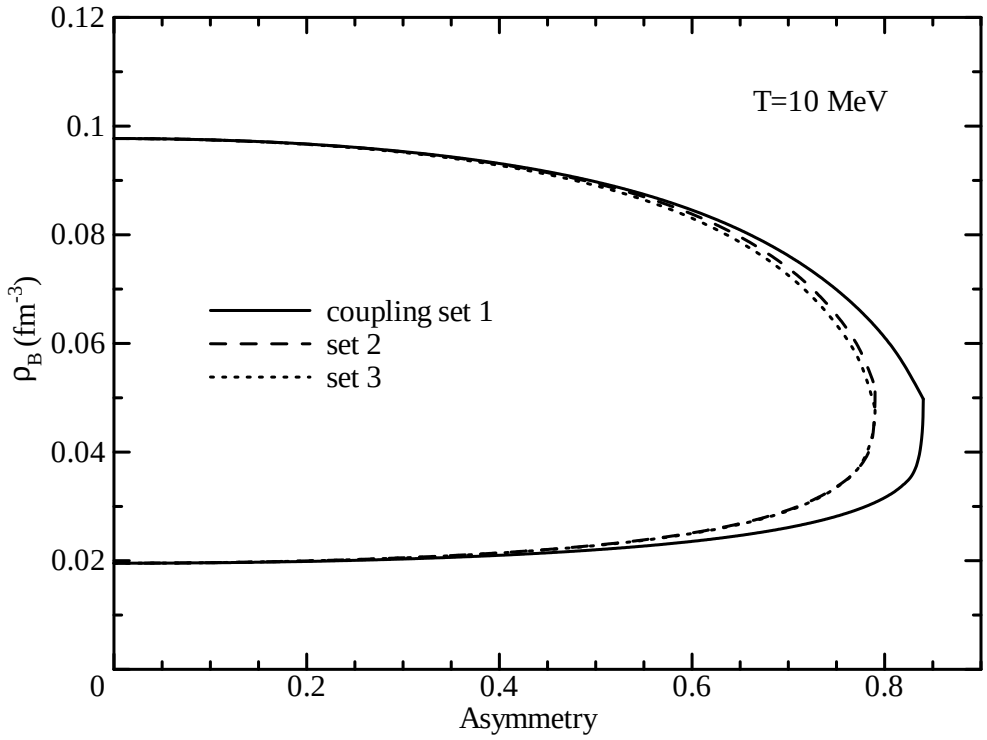

Figure 4: The spinodal regions in the density-asymmetry plain for the three sets of isovector meson coupling constants at $T = 10\,\mathrm{MeV}$. The solid curve is calculated using the coupling constants $(g_{NN\delta}/m_\delta)^2 = 0.39\,\mathrm{fm}^2$ and $(g_{NN\rho}/m_\rho)^2 = 0.82\,\mathrm{fm}^2$ (set 1) from Bonn A potential of Ref. [17]. The dashed and dotted curves are calculated using $(g_{NN\delta}/m_\delta)^2 = 0.39\,\mathrm{fm}^2$ and $(g_{NN\rho}/m_\rho)^2 = 1.432\,\mathrm{fm}^2$ (set 2), and $(g_{NN\delta}/m_\delta)^2 = 1.0\,\mathrm{fm}^2$ and $(g_{NN\rho}/m_\rho)^2 = 1.888\,\mathrm{fm}^2$ (set 3).

stronger isovector repulsive potential than the set 1 at large asymmetry. The stronger repulsion produces more disordered system. Then, the unstable spinodal region becomes smaller at large asymmetry. Although the stronger $NN\delta$ coupling in the set 3 requires the much stronger $NN\rho$ coupling to reproduce the same symmetry energy as the set 2 [12], the large cancellation between the attractive scalar and repulsive vector potentials produces the same net result of spinodal region in the set 3 as the set 2.

Finally, we return to Fig. 3 and compare it with the spinodals in Fig. 4 of Ref. [9] by the NLW model. Even if the difference of the symmetry energy is considered, the EZM model produces longer and wider spinodal region than the NLW model. The result is due to the renormalized vector-meson coupling constants (8)-(11). The renormalized $NN\omega$ coupling constant is reduced from its free value at larger isoscalar density ρ_B. This means that the isoscalar repulsive potential becomes weaker. Consequently, the upper-density boundary of the spinodal region in the EZM model shifts to higher density in comparison with the NLW model. (The lower-density boundary is not altered largely because the reduction of the renormalized coupling constant is little at low density.) Similarly, the renormalized $NN\rho$ coupling constant is reduced from its free value at larger isovector

density or asymmetry. This means that the isovector repulsive potential becomes weaker. Consequently, at finite temperature the maximum asymmetry of the spinodal region in the EZM model shifts to higher asymmetry as compared with the NLW model.

We have investigated the unstable spinodal region of asymmetric nuclear matter in the extended Zimanyi-Moszkowski model, which reproduces well the saturation properties and the critical phenomena of symmetric nuclear matter. It is found that the maximum asymmetry of the spinodal region shifts to lower value for higher symmetry energy. On the other hand, for a fixed symmetry energy the differences of the isovector coupling constants have little effect on the spinodal region. It is also found that at a fixed temperature the EZM model produces larger spinodal region in the density-asymmetry plain, higher upper-density boundary and maximum asymmetry, than the familiar NLW model because of the renormalized vector-meson coupling constants.

References

[1] Y.G. Ma *et al.* Phys. Rev. **C71** (2005) 054606, [arXiv:nucl-ex/0410018] and references therein.

[2] B. Borderie *et al.* Nucl. Phys. **A734** (2004) 495, [arxiv:nucl-ex/0311016].

[3] V.A. Karnaukhov *et al.* Nucl. Phys. **A749** (2005) 65, [arXiv:nucl-ex/0410017].

[4] P. Chomaz, M. Colonna and J. Randrup, Phys. Rep. **389** (2004) 263.

[5] H. Műller and B. D. Serot, Phys. Rev. **C52** (1995) 2072, [arXiv:nucl-th/9505013].

[6] B.A. Li and C.M. Ko, Nucl. Phys. **A618** (1997) 498, [arXiv:nucl-th/9701049].

[7] B. Liu, V. Greco, V. Baran, M. Colonna and M. Di Toro, Phys. Rev. **C65** (2002) 045201, [arXiv:nucl-th/0112034].

[8] J. Margueron and P. Chomaz, Phys. Rev. **C67** (2003) 041602, [arXiv:nucl-th/0212082].

[9] S.S. Avancini, L. Brito, D.P. Menezes and C. Providência, Phys. Rev. **C70** (2004) 015203, [arXiv:nucl-th/0406022].

[10] W. Zuo, Z.H. Li, A. Li and U. Lombardo, Nucl. Phys. **A745** (2004) 34, [arXiv:nucl-th/0412101].

[11] B.D. Serot and J.D. Walecka, *Advances in Nuclear Physics*, Vol. **16** (Plenum, New York, 1986).

[12] S. Kubis and M. Kutschera, Phys. Lett. **B399** (1997) 191, [arXiv:astro-ph/9703049].

[13] J.B. Natowitz *et al.* Phys. Rev. Lett. **89** (2002) 212701, [arXiv:nucl-ex/0204015].

[14] K. Miyazaki, Mathematical Physics Preprint Archive (mp_arc) 05-178.

[15] K. Miyazaki, Mathematical Physics Preprint Archive (mp_arc) 05-261.

[16] K. Miyazaki, Mathematical Physics Preprint Archive (mp_arc) 05-190.

[17] R. Brockmann and R. Machleidt, Phys. Rev. **C42** (1990) 1965.